Effective single-particle order-N scheme for the dynamics of open non-interacting many-body systems

Yu. V. Pershin, Y. Dubi and M. Di Ventra
Department of Physics, University of California San Diego, La Jolla, California 92093-0319, USA

Quantum master equations are common tools to describe the dynamics of many-body systems open to an environment. Due to the interaction with the latter, even for the case of non-interacting electrons, the computational cost to solve these equations increases exponentially with the particle number. We propose a simple scheme, that allows to study the dynamics of N non-interacting electrons taking into account both dissipation effects and Fermi statistics, with a computational cost that scales linearly with N. Our method is based on a mapping of the many-body system to a specific set of effective single-particle systems. We provide detailed numerical results showing excellent agreement between the effective single-particle scheme and the exact many-body one, as obtained from studying the dynamics of two different systems. In the first, we study optically-induced currents in quantum rings at zero temperature, and in the second we study a linear chain coupled at its ends to two thermal baths with different (finite) temperatures. In addition, we give an analytical justification for our method, based on an exact averaging over the many-body states of the original master equations.

PACS numbers: 03.65.Yz, 72.10.Bg

I. INTRODUCTION

Quantum systems that exchange energy with an environment have attracted a great deal of attention for many years[1,2]. The interest in these dissipative (open) quantum systems ranges from quantum computing and quantum information theory to biological physics[3]. Recent developments in the transport properties of nanoscale systems[4] raise new interest in these topics. For instance, the dissipative effects of the surrounding environment are key to understand the non-equilibrium properties of nanostructures and their approach to steady state[5]. However, the study of dissipative many-body quantum systems represents a major computational challenge.

There are essentially two ways to approach this problem. One consists in deriving equations of motion (master equations) for the reduced density matrix (DM) of the system of interest by integrating out the degrees of freedom of the bath.[6] The further assumption of Markovian dynamics leads to different kinds of master equations for the DM[7], perhaps the most popular being the Lindblad equation[8] which is often used in quantum optics[9,10]. The second approach is to use stochastic Schrödinger equations[7,10] which are the stochastic unraveling of the master equations. If the Hamiltonian of the system does not depend on microscopic degrees of freedom, like the density or current density, both approaches describe the same physical properties.[11]

Irrespective of the chosen method, the solution of these equations is a formidable task which scales exponentially with the number of electrons. This is true even for a system of non-interacting electrons since the correlations induced by the bath make it impossible to exactly reduce the N-particle equation of motion into N distinct single-particle equations of motion. It is the goal of this paper to discuss an *ansatz* which greatly simplifies this task for the dynamics of N non-interacting electrons in interaction with a bath. We focus on the DM approach but the conclusions are exactly the same for the stochastic Schrödinger equations. The latter, in fact, have found application in the recently developed stochastic time-dependent current-density functional theory (S-TDCDFT)[11], an extension of time-dependent current-density functional theory to systems in dynamical interaction with an environment. In S-TDCDFT the many-body interacting problem in the presence of the environment is mapped into an effective single-particle non-interacting problem in the presence of the same environment. The *ansatz* we discuss in this work is thus of great use in the numerical solution of the equations of motion of S-TDCDFT,[11] and may therefore find application in disparate problems beyond the examples presented in this paper, where interactions are important.

The outline of the paper is as follows. In Sec. II we describe in detail our proposed scheme. We define the master equation framework and our *ansatz*, along with the detailed structure of the resulting equations. In Secs. III and IV we give numerical examples of our scheme. We calculate currents induced by optical excitation in quantum ring structures in the presence of dissipation at $T = 0$ (Sec. III) and consider steady state properties of a quantum system at finite temperatures (Sec. IV). We study systems which are small enough so that we can compare the results from our scheme with the full many-body calculation. We find excellent agreement between the two methods for a large range of parameters. In Sec. V we derive an analytical justification for our scheme. Starting from the exact many-body master equations we average over the many-body degrees of freedom and study the resulting (non-linear) equations. Sec. VI is devoted to a summary and outlook.

II. CALCULATION SCHEME

Our goal is to study the dynamics of N electrons described by a non-interacting Hamiltonian $\mathcal{H} = \sum_j H_j$, while taking into account dissipation processes. To be more specific let us employ the following Lindblad-type master equation for the many-electron DM ρ_M ($\hbar = 1,\ e = 1$)[8]

$$\dot{\rho}_M = -i[\mathcal{H}, \rho_M] + \mathcal{L}\rho_M \quad , \tag{1}$$

where $[\cdot]$ denotes the commutator, and $\mathcal{L}$ is the Lindbladian superoperator, defined via a set $V_{nn'}$ of so-called "Lindblad operators" by

$$\mathcal{L}\rho_M = \sum_{n,n'} \left(-\frac{1}{2}\{V_{nn'}^\dagger V_{nn'}, \rho_M\} + V_{nn'}\rho_M V_{nn'}^\dagger \right) \quad , \tag{2}$$

with $\{\cdot\}$ the anti-commutator. The sums over n and n' ($n \neq n'$) are performed over all many-particle levels of the system and the V-operators are conveniently selected in the form $V_{nn'} = \sqrt{\gamma_{nn'}}|\Psi_n\rangle\langle\Psi_{n'}|$, describing a transition from the many-body state $|\Psi_{n'}\rangle$ into the state $|\Psi_n\rangle$ with the transition rate $\gamma_{nn'}$. Although $\gamma_{nn'}$ are introduced phenomenologically here, these coefficients can be in principle derived from a microscopic theory.

A common form for $\gamma_{nn'}$ is described as follows[12]. At $T = 0$, dissipation drives the system towards its ground state, which we denote by the index $n = 1$. Therefore, it is reasonable to select $\gamma_{nn'} = 0$ for $n > 1$. Moreover, by assuming that the transition rate into the ground state is independent of n' , we may write $\gamma_{1,n'} = \gamma$. This choice for the relaxation rates is a $T = 0$ manifestation of detailed balance[7], which we assume to hold for a Markovian ohmic bath in the long-time limit. In fact, there are other ways to choose the relaxation operators and still ensure detailed balance, and we have checked different options in our numerical calculations (Sec. III) and found no qualitative change in our results. Therefore, we shall keep the above normalization hereon.

For a system with M single-electron energy levels and N electrons, the solution of Eq. (1) generally requires the solution of $(C_N^M + 2) \times (C_N^M - 1)/2$ coupled differential equations, where $C_N^M = M!/N!(M-N)!$ and we have taken into account constrains of hermiticity and the unit trace of the density matrix. For the general case (excluding, e.g., $N = 1$ or $N = M$), the problem thus scales exponentially with the number of particles[13].

Consider now an operator $A = \sum_j A_j$, a sum over single-particle operators. (This is not the most general form of operator but it encompasses most of the observables of physical interest, like, e.g., the density or current density.) We make the following conjecture: the expectation value of A over a many-particle non-interacting electron state with dissipation can be approximated as a sum of single-electron expectation values of A_j over an ensemble of N single-electron systems with *specifically selected* single-electron dissipation operators, i.e.

$$\mathrm{Tr} A\rho_M \simeq \sum_{j=1}^{N} \mathrm{Tr} A_j \rho^{(j)}. \tag{3}$$

Here, $\rho^{(j)}$ is a single-electron DM (effectively describing the j-th electron), each obeying its own Lindblad master equation

$$\dot{\rho}^{(j)} = -i[H_j, \rho^{(j)}] + \mathcal{L}^{(j)}\rho^{(j)} \quad . \tag{4}$$

The choice of superoperators $\mathcal{L}^{(j)}$ is dictated by two requirements: (i) for a time-independent Hamiltonian the dissipation processes should result in the Fermi-Dirac distribution at long times, and (ii) the relaxation rate of many-electron states is γ.

As we will demonstrate (numerically in Sec. III as well as analytically in Sec. V), these two requirements are met if one chooses a simple form for the V-operators, which reflects the physical process at which the different electrons decay to consecutive single-particle levels (i.e., the $i-$th electron will decay to the i-th single-particle level, see Eq. (5)). Once a form for $\mathcal{L}^{(j)}$ is chosen, one only needs to solve $\sim N \times M^2$ equations, a reduction which enormously speeds up numerical calculations.

The simplest choice for the Lindbladian superoperator which satisfies the above criteria is similar to the one in Eq. (2), with single-electron V operators of the following form: for the j-th electron we select at $T = 0$

$$V_{kk'}^j = \begin{cases} \sqrt{\gamma}|j\rangle\langle k'| & , \quad k' \neq k = j; \quad k \leq k_F \\ 0 & , \quad \text{otherwise} \end{cases} \quad , \tag{5}$$

where $|k\rangle$ are now the single-particle states and k_F is the index of the Fermi level. In some sense, such a replacement of the many-body equation of motion by a set of auxiliary single-electron equations is similar to the introduction of a fictitious system of non-interacting electrons in density-functional theory.[11]

To summarize our scheme, it is constructed from the following steps: (i) given a non-interacting Hamiltonian, one constructs a set of Lindblad operators (following Eq. (2) and Eq. (5)), (ii) a set of single-particle density matrices $\rho^{(j)}$ is defined, and corresponding master equations [Eq. (4)] are solved, and, finally, (iii) any observable quantity (made of quadratic operators in the second quantization formalism) can be calculated using Eq. (3).

III. NUMERICAL DEMONSTRATION: DRIVEN SYSTEM AT $T = 0$

In order to test the conjecture (3), we have performed extensive numerical calculations considering a driven quantum system in a wide range of parameters. We found that for a system with non-degenerate levels Eq. (3) is almost perfectly satisfied. We believe that in systems with degenerate energy levels a deviation from

Eq. (3) is due to the intrinsic ambiguity of degenerate states.

We consider a system of N tight-binding electrons on both a ring and a double ring of M sites in the presence of circularly-polarized electromagnetic radiation (see insets in Fig. 1). In order to lift the degeneracy, we place the system in a weak magnetic flux. The Hamiltonian of the system is given by

$$\mathcal{H} = -t\sum_i \left(e^{i2\pi\phi/\phi_0}c_i^\dagger c_{i+1} + h.c.\right) + \sum_i U_i(t)c_i^\dagger c_i \quad . \quad (6)$$

Here t is the hopping integral (we set $|t| = 1$ throughout the calculation) and $U_i(t) = -e\mathbf{E}(t)\cdot\mathbf{r}_i$ is a change of the potential energy of the i-th site ($\mathbf{r}_i$ is its position) due to the external radiation. The magnetic field is taken into account via the usual Peierls substitution, with ϕ the magnetic flux through the ring, and $\phi_0 = h/e$ the flux quantum. The electric field is written as $\mathbf{E}(t) = E_0\cos(\omega t)\hat{\mathbf{x}} \pm E_0\sin(\omega t)\hat{\mathbf{y}}$, where E_0 and ω are the electric field amplitude and frequency, $\hat{\mathbf{x}}$ and $\hat{\mathbf{y}}$ are unit vectors in the x and y directions (in the ring plane), and $\pm$ corresponds to a $\sigma_\pm$ circular polarization.

It is known that in the ring topology a circularly-polarized radiation creates a current in the ring[14,15]. We calculate the expectation value of the current operator through a specific bond, $J = \frac{ie}{\hbar}\langle c_i^\dagger c_{i+1} - h.c.\rangle$, using both the exact many-body DM, and a set of single-electron density matrices calculated as described above.[16] In both schemes we start by diagonalizing the tight-binding part of the Hamiltonian. In the many-body (exact) scheme, we then write the time-dependent potential and the Lindblad operators in their full many-body form and solve the time-dependent set of equations for the many-body DM. For the single-particle scheme, we solve a set of N single-particle Lindblad equations (of size $M \times M$), each with its own set of relaxation operators $\mathcal{L}^{(j)}$. The current is then calculated as a function of time using the LHS (many-body form) and the RHS (single-particle form) of Eq. (3). The calculations were made for a wide range of system parameters, displaying excellent agreement between the two schemes.

A. Ground-state initial conditions

Fig. 1 shows the current calculated by the two methods through a bond connecting two adjacent sites of a 10-site ring containing 3 electrons. We see that the current through the bond oscillates in agreement with a previous study[15]. Most importantly, in the context of the present investigation, the current values hardly differ between the two schemes. The average deviation of the two currents is less then 1.5% (the maximum deviation is $\approx 6.5\%$). This difference rapidly disappears with decreasing E_0. This is seen from comparing Fig. 2(a) and 2(b) where the current excited in a double ring structure is plotted for two different values of the electric field

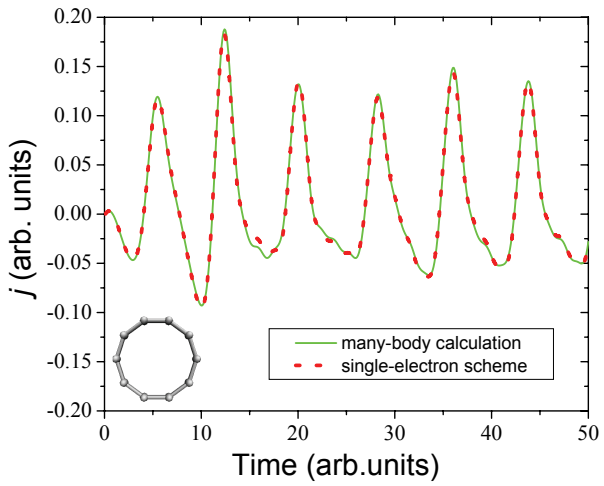

FIG. 1: (Color online) Current between two sites of a ring as a function of time calculated by the exact many-body and approximate single-electron approaches. Inset shows the system geometry. This calculation has been done with the following set of parameters: $N = 3$, $M = 10$, $eE_0a = 0.1$, $\omega = 0.8$, $\sigma = 1$, $\gamma = 0.1$, $a = 0.1415$nm and $B = 10$T. a is a bond length. The magnetic field corresponds to a flux through the ring of $\phi/\phi_0 \approx 1.66 \times 10^{-4}$.

amplitude, $eE_0a = 0.1$ and $eE_0a = 0.01$, respectively. One clearly sees that the discrepancies between the two methods (marked in a gray circle in 2(a)) diminish as the excitation field decreases. The results presented in Figs. 1 and 2 were obtained assuming that at time $t = 0$ the system is in its ground state.

B. Non-equilibrium initial conditions

Next, we have tested the applicability of our approach to highly excited states. In Fig. 3 we plot the current gnerated in a 10-site ring containing 3 electrons. The difference with previously discussed calculations is that now we assume that in the initial moment of time the system is in its highest energy state. For a single electron, there are 10 energy states in the 10-site ring. We made calculations considering different relaxation schemes. Indeed, there is an arbitrariness in the relaxation state assignment (e.g., V operators for the electron which is initially in the 10-th state – highest energy state – can be selected to describe its relaxation into the first, second or third lowest energy state). Fig. 3 displays a very good agreement of the many-body calculation compared to the results obtained using our single-electron approach with two different relaxation schemes. Importantly, since the rates at which electrons relax into their ground states are the same, the two relaxation schemes lead to the same current, showing the insensitivity of our general scheme to the details in the initial state de-population. Also, in the long-time limit the current is independent of the initial conditions chosen (cf. the current in Fig. 3 with the

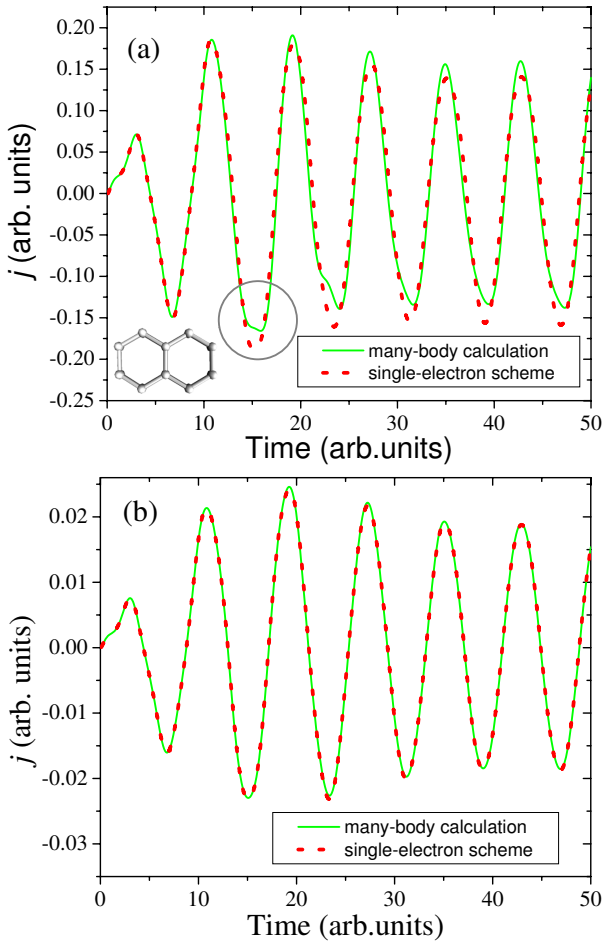

FIG. 2: (Color online) Current excited in a double ring calculated by the exact many-body and approximate single-electron approaches. The electric field amplitude is (a) $eE_0a = 0.1$ and (b) $eE_0a = 0.01$. All other parameters are the same as in Fig. 1. The system geometry is shown in the inset of (a). The discrepancies between the two methods (such as marked in a gray circle in (a)) diminish as the excitation field decreases.

current in Fig. 1 at $t > 40$).

C. Precision of the simplified scheme

In order to study the precision of the single-electron scheme, we calculate the current excited in a 6-site ring containing 3 electrons. Our main observation is that the simplified scheme provides a very good precision for the whole range of parameters used in the calculations. We have found that a slightly better precision is obtained at weak and strong electric fields. This particular observation is clearly seen in Fig. 4 where we plot the ratio of the RMS of current differences calculated as

$$\Delta j_{rms} = \frac{1}{\tau}\int_0^\tau \sqrt{(j_{mb} - j_{se})^2}\,dt \qquad (7)$$

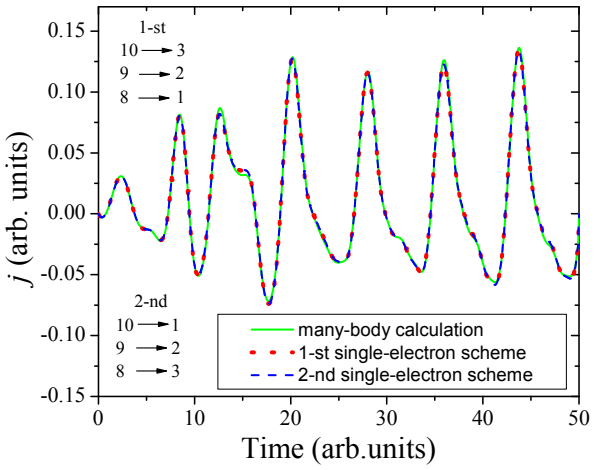

FIG. 3: (Color online) Comparison of many-body calculations with those obtained with the simplified approach in the case of non-equilibrium initial conditions. For single electron calculations, we used two different relaxation schemes shown as insets. This plot was obtained for a 10-site quantum ring using the same parameter values as in Fig. 1.

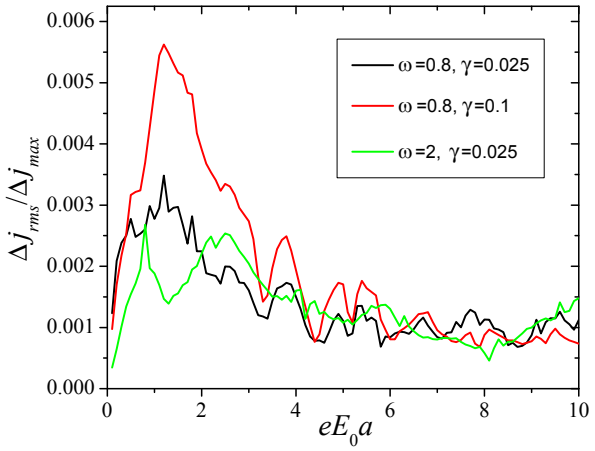

FIG. 4: (Color online) RMS of the difference of currents calculated by many-body and single-electron schemes divided by the maximum current amplitude within the calculation time as a function of the electric field amplitude. This plot was obtained for $N = 3$, $M = 6$, $\sigma = 1$, $a = 0.1415$nm, $B = 10$T and $\tau = 100$. The other calculation parameters are shown in the figure.

to $\Delta j_{max} = j_{mb}^{max} - j_{mb}^{min}$. Here, τ is a sampling period, $j_{mb(se)}$ is the current calculated using many-body (single-electron) scheme and $j_{mb}^{max(min)}$ is the maximum (minimum) value of current calculated within the time interval $[0, \tau]$. A better agreement at weak fields can be related to the fact that in this situation only the low-energy states become occupied and the relaxation operators in the many-electron and single-electron schemes are the same (see Sec. V for more arguments). At strong fields, the better agreement is due to the fact that the

electric field term is dominant in the equations of motion. Fig. 4 also demonstrates that the single-electron scheme precision slightly depends on simulation parameters and is a better approximation when dissipation is weaker.

Fig. 5 presents selected results of our calculations showing agreement between many-body and single-electron calculations at several values of the electric field amplitude. The interesting feature of these results is that at weak driving fields the single-electron scheme precision is better at longer times ($t \gtrsim 60$ in Fig. 5(a)), at intermediate fields the scheme precision is better in the initial time interval ($t \lesssim 20$ in Fig. 5(b)) and at strong fields the precision is better again at longer times (Fig. 5(c)).

IV. NUMERICAL DEMONSTRATION: STEADY STATE AT FINITE TEMPERATURES

In the second numerical example, we study a non-equilibrium system at finite temperatures. The system of interest is a linear metallic chain, connected at its two ends to two thermal baths at different temperatures, T_L and T_R, corresponding to the left and right temperatures (see inset of Fig. 6(b)).

The Hamiltonian of the system is given by $\mathcal{H} = -t\sum_{\langle i,j\rangle\in L,R,d}\left(c_i^\dagger c_j + h.c.\right)$ (t is the hopping integral, which serves as the energy scale, and we have chosen $t = 1$). The master equation now takes the form

$$\dot{\rho} = -i[\mathcal{H},\rho] + \mathcal{L}_L[\rho] + \mathcal{L}_R[\rho] \tag{8}$$

where $\mathcal{L}_{L(R)}$ describes relaxation processes due to the contact between the left (right) lead with its respective bath at temperature $T_{L(R)}$. The V-operators are given by

$$V_{kk'}^{(L,R)} = \sqrt{\gamma_{kk'}^{(L,R)} f_D^{(L,R)}(\epsilon_k)}|k\rangle\langle k'| \quad , \tag{9}$$

where $f_D^{(L,R)}(\epsilon_k) = 1/\left(\exp\left(\frac{\epsilon_k-\mu}{k_B T_{L,R}}\right)+1\right)$ are the Fermi distributions of the left and right leads, with μ the chemical potential. The coefficients

$$\gamma_{kk'}^{(L,R)} = |\psi_k(r)\,\gamma_0\,\psi_{k'}^*(r)|_{r=r_L(r_R)} \tag{10}$$

describe the overlap between the single-particle states $|k\rangle$ and $|k'\rangle$ over the point of contact $r_{L(R)}$ between the left (right) baths and the corresponding junction leads. The constant γ_0 describes the strength of interactions between the bath and electrons. The form (10) can be derived from first principles by tracing out the bath degrees of freedom, with the latter formed by a *dense* spectrum of boson excitations (e.g., phonons), which interact locally with electrons at the edges of the system. Physically, it corresponds to the experimental situation in which the left (right) bath induces energy relaxation only between states which reside predominantly on the left (right) edge of the junction, where the bath is in contact. The operators (9) guarantee that the system evolves to a global equilibrium if $T_L = T_R$. For $T_L \neq T_R$ this system is inherently out of equilibrium, and reaches a steady state which may have, for instance, a non-uniform electron density[17], and is thus relevant for experiments of thermo-power measurements in nano-systems[18]. We point out that the above model also relaxes the con-

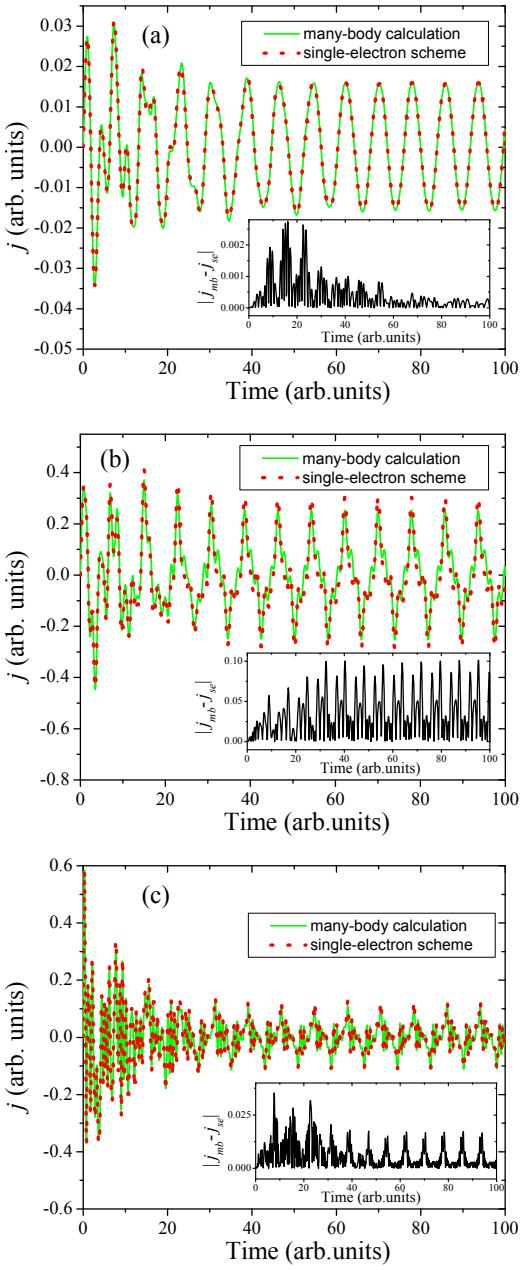

FIG. 5: (Color online) Current excited in a 6-site ring calculated by different approaches as indicated. The calculation parameters are the same as in Fig. 4. The electric field amplitude is $eE_0a = 0.1$ (a), 1.7 (b) and 8 (c). The insets show the absolute value of many-body (j_{mb}) and single-electron (j_{se}) currents difference as a function of time.

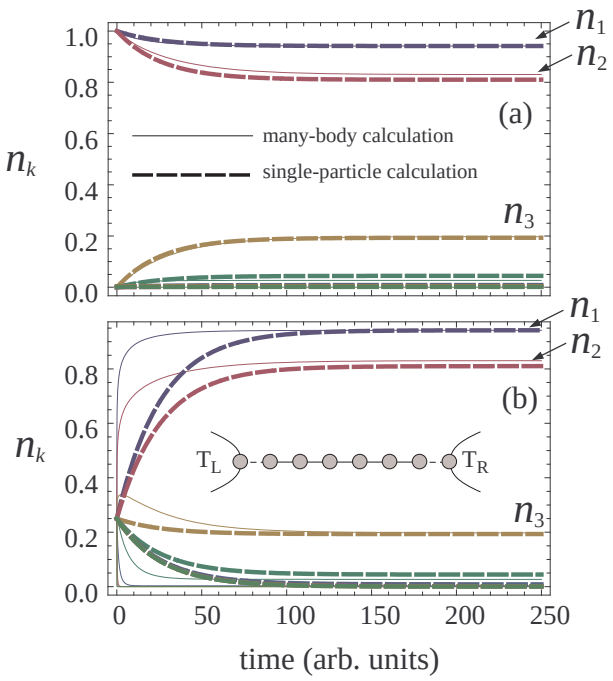

FIG. 6: (Color online) Occupation of the different single-particle energy levels as a function of time for the two calculation schemes, the full many-body calculation (solid lines) and the approximate scheme (dashed lines). Initial condition are either (a) the ground state or (b) a uniformly-occupied state. The chain length is $L = 12$, with the parameters $g = 1$, $\gamma_0 = 0.01$, $T_L = 0.1$ and $T_R = 0.4$.

straint of Sec. III that there is a single relaxation rate for all relaxation processes.

In Fig. 6 we plot the occupation of the different single-particle energy levels as a function of time for the two calculation schemes, the full many-body (solid lines) and the approximate scheme (dashed lines). The chain length is $L = 12$, with the parameters $g = 1$, $\gamma_0 = 0.01$, $T_L = 0.1$ and $T_R = 0.4$, and it is occupied by two electrons. We have plotted the dynamics starting from either the ground state (Fig. 6(a)) or a uniform state, where all energy levels are equally occupied (Fig. 6(a)). As seen, starting from the ground state (Fig. 6(a)) there is excellent agreement between the two schemes both in the transient dynamics and in the steady state. On the other hand, if we start from an excited state (Fig. 6(b)) then the transient dynamics exhibit slight differences between the exact and approximate scheme. The steady state is, naturally, the same with either initial conditions. Similar calculations with different parameters have yielded similar results.

In order to study the accuracy of the approximation also in the present example, we calculate the difference in the local density between the two schemes, $\Delta n_i = |n_{i,mb} - n_{i,sp}|$, at steady state. Here, $n_{i,mb(sp)}$ is the local density ($n_i = \sum_k |\psi_k(i)|^2 \rho_{kk}$) at the i-th site, calculated with the many-body (single-particle) scheme. In Fig. 7 we plot Δn (averaged over the entire chain),

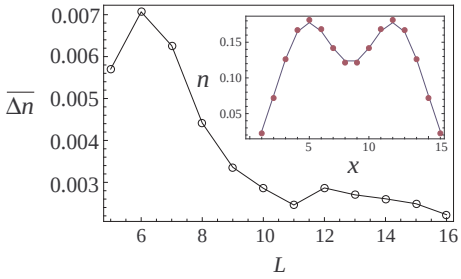

FIG. 7: (Color online) Difference in the local density $\overline{\Delta n}$ (averaged over the entire chain) as a function of system length at steady state. The numerical parameters are the same as in Fig. 6. Inset : local density along a $L = 16$ chain, calculated using the exact scheme (points) and approximate scheme (solid line).

for the same parameters as in Fig. 6 for different chain lengths $L = 5, 6, ..., 16$. We find that as the system becomes larger the approximation improves (the relative deviation for the larger systems is less than 3%). The reason for the improvement of the approximation with increasing length stems from the fact that as the system becomes larger, the single-particle occupations of the many-body system become closer and closer to a true broadened Fermi distribution. In the inset of Fig. 7 we plot the local density along a $L = 16$ chain, calculated using the exact scheme (points) and approximate scheme (solid line), showing the excellent agreement between the two.

V. ANALYTIC JUSTIFICATION

We now provide an analytical argument for the validity of our *ansatz* , which is summarized in Eqs. (3-5) for $T = 0$. In order to do so we start from the definition of an auxiliary single-particle density matrix (SPDM) from the many-body one. We then evaluate its equation of motion by summing up the many-body degrees of freedom, and study the structure of the equations. We in fact find that this SPDM can be approximately written as sum of single-particle density matrices obeying equations of motion with specific bath operators, thus validating our *ansatz*. We do this for finite temperatures, and show that the result leads to the $T = 0$ form for the relaxation operators used in the numerical calculations.

Let us define the following SPDM

$$\rho(t) = \sum_{kk'} \rho_{kk'}(t) |k\rangle\langle k'| \ . \tag{11}$$

The matrix elements are derived from the many-body DM by

$$\rho_{kk'} = \mathrm{Tr}\left(c_k^\dagger c_{k'} \rho_M\right) . \tag{12}$$

We show below that $\rho(t)$ can be approximated as

$$\rho(t) \simeq \sum_j \rho^{(j)}(t), \tag{13}$$

where $\rho^{(j)}$ are the single-particle density matrices entering Eq. (3).

The time evolution of the SPDM is determined by

$$\dot{\rho}_{kk'} = \frac{\mathrm{d}}{\mathrm{d}t}\mathrm{Tr}\left(c_k^\dagger c_{k'}\rho_M\right) = \mathrm{Tr}\left(c_k^\dagger c_{k'}(-i[\mathcal{H},\rho_M] + \mathcal{L}\rho_M)\right). \tag{14}$$

One can now perform the trace exactly using Wick's theorem. The relaxation operators $V_{nn'}$ defined below Eq. (2) generally involve up to M creation and M annihilation operators. Therefore, it is not practical to use them in analytical calculations. We instead consider V operators of a commonly used[19] simplified form $V_{kk'} = (\gamma_{kk'})^{\frac{1}{2}}\, c_k^\dagger c_{k'} \quad , k \neq k'$. It is clear that when excitation of the system is weak, and highly excited states are almost unpopulated, the physical effect caused by both operators is nearly the same. Note, however, that taking this form for the V-operators (which excludes direct relaxation of highly-excited states into the ground state) does not lead to a reduction in the number of equations needed to be solved, since the equations remain fully coupled (put it differently, the Lindbladian operator cannot be subdivided into blocks).

A. Diagonal elements

We start by deriving equations of motion for the diagonal elements of the SPDM. For the sake of simplicity, let us assume that the system Hamiltonian is time-independent and diagonalized. Then, it is easy to find that the equations of motion for the diagonal elements of the SPDM are[20]

$$\begin{aligned}\dot{\rho}_{kk} \;=\; & -\frac{1}{2}\sum_{k'\neq k}\gamma_{kk'}\rho_{kk} + \frac{1}{2}\sum_{k'\neq k}\gamma_{k'k}\rho_{k'k'} + \\ & + \frac{1}{2}\rho_{kk}\sum_{k'\neq k}(\gamma_{k'k} - \gamma_{kk'})\rho_{k'k'}.\end{aligned} \tag{15}$$

Let us examine Eq. (15) by making two assumptions: (i) the coefficients are only a function of the first index, i.e., $\gamma_{kk'} = \gamma_{k'}$, and (ii) the third (non-linear) part on the RHS of Eq. (15) is negligible and is set to zero. Within these assumptions, and noting that by definition $\sum_{k=1}^{M}\rho_{kk} = N$, one obtains the equation

$$\dot{\rho}_{kk} = -Z\rho_{kk} + \gamma_k(N - \rho_{kk}), \tag{16}$$

where $Z = \sum_{k'\neq k}\gamma_{k'}$. Solving this equation yields

$$\rho_{kk}(t) = \left(\rho_{kk}(0) - \frac{\gamma_k N}{\gamma_k + Z}\right)\epsilon^{-(Z+\gamma_k)t} + \frac{\gamma_k N}{\gamma_k + Z}. \tag{17}$$

For a Fermi system, the long-time limit of the SPDM should be $\rho_{kk}(t\to\infty) = f_D(\epsilon_k)$, where $f_D(\epsilon_k) = 1/(1+\exp((\epsilon_k-\mu)/k_BT)$ is the Fermi-Dirac distribution. It follows directly that in order to satisfy this long-time limit, the coefficients must be chosen such that $\gamma_k = \gamma f_D(\epsilon_k)$.

We now turn back to the third, non-linear part in the RHS of Eq. (15). Keeping in mind the definition for γ_k, this part now reads $\gamma\rho_{kk}\sum_{k'\neq k}(f_D(\epsilon_k) - f_D(\epsilon_{k'}))\rho_{k'k'}$. In the long-time limit, as ρ_{kk} approach their equilibrium values, and at zero temperature, one can consider two possibilities. In the first, both k and k' lie below or above the Fermi surface. In this case, $f_D(\epsilon_k) - f_D(\epsilon_{k'}) \approx 0$ and the non-linear part vanishes. If, on the other hand, either k or k' lie below the Fermi surface and the other above it, then indeed $f_D(\epsilon_k) - f_D(\epsilon_{k'}) \neq 0$. However, in that case either $\rho_{kk} \approx 0$ or $\rho_{k'k'} \approx 0$. Thus, in the low temperature long-time limit, the third term on the RHS of Eq. (15) is negligible, which means that our assumption (ii) above is justified.

Extending this conclusion to finite temperatures and to all times, we end up with a simple equation for the diagonal elements of the SPDM,

$$\rho_{kk} = -\gamma\sum_{k'\neq k} f_D(\epsilon_{k'})\rho_{kk} + \gamma\sum_{k'\neq k} f_D(\epsilon_k)\rho_{k'k'}. \tag{18}$$

Simple algebra reveals that these equations are equal to those obtained from applying the Lindbladian operator, Eq. (2), to the SPDM, with the V-operators having the form

$$V_{kk'} = \sqrt{\gamma f_D(\epsilon_k)}|k\rangle\langle k'| \quad , \tag{19}$$

which is a particular case of the operators (9), thus justifying their structure. We thus propose that the SPDM evolves according to Eq. (1) and (2), with the Lindblad operator given in terms of Eq. (19).

The equations of diagonal SPDM elements can be derived differently. Since $\rho(t) \simeq \sum_j \rho^{(j)}(t)$, using Eq. (4) with the single-electron V-operators in the form

$$V^j_{kk'} = \delta_{kj}(1-\delta_{kk'})\sqrt{\gamma f_D(\epsilon_k)}|j\rangle\langle k'|, \tag{20}$$

we can obtain a set of equations which is the same as Eq. (15). This demonstration clearly shows a similarity of our single-electron and many-body approaches. Note, that the definition (20) coincides with Eq. (5) at $T = 0$. Moreover, while there is no *a priori* justification for neglecting the non-linear terms, the numerical calculations of the previous sections show that it is an excellent approximation for non-interacting systems.

Let us also point out that the equations for the diagonal and off-diagonal parts of the SPDM are completely decoupled (this result is exact). Therefore, if one is interested in the time-dependent expectation value of an operator that commutes with the Hamiltonian, or only in the steady-state (where the off-diagonal elements vanish) our *ansatz* reduces the computational effort to a single $M \times M$ equation for the diagonal elements of the SPDM.

B. Off-diagonal elements

The off-diagonal elements of the density matrix are needed to calculate, e.g., local currents or densities in a non-equilibrium situation of an excited system (as in the numerical examples of Sec. III). As stated above, if only the diagonal elements are of interest, SPDM calculations with the V-operators in their especially simple form (Eq. 19) can be used. If the off-diagonal elements are important, calculations using single-electron matrices ρ^j with relaxation operators given by Eq. 20 have to be performed.

In order to understand why single-electron calculations are needed (or why SPDM does not provide the best results in all cases), we study the equation of motion for the off-diagonal elements of the exact Lindblad operator. Using Eq. (14) and $V_{kk'}$ operators defined below Eq. (14) one finds

$$(\mathcal{L}\rho)_{kk'} = -\frac{1}{2}\sum_{k''\neq k,k'}(\gamma_{k''k'}+\gamma_{k''k})(1-\rho_{k''k''})\rho_{kk'} - \\ -\frac{1}{2}\sum_{k''\neq k,k'}(\gamma_{kk''}+\gamma_{k'k''})\rho_{kk'}\rho_{k''k''}. \quad (21)$$

Again we make the substitution $\gamma_{kk'} = \gamma f_D(\epsilon_{k'})$, and consider for simplicity the system at zero temperature. By assuming $\rho_{kk} \approx f_D(\epsilon_k)$ we find that the first element of the LHS in Eq. (21) is negligible, and one is left with

$$(\mathcal{L}\rho)_{kk'} \approx -\frac{\gamma}{2}\sum_{k''\neq k,k'}\rho_{k''k''}\rho_{kk'} = -\frac{\gamma}{2}(N-\rho_{kk}-\rho_{k'k'})\rho_{kk'}. \quad (22)$$

If one uses SPDM calculations to study the off-diagonal elements, then one finds that $(\mathcal{L}\rho)_{kk'}$ does not depend on ρ_{kk}, $\rho_{k'k'}$ at all. However, within the single-electron scheme this separation can not be made, and the dynamics of the off-diagonal elements are better captured. This can be seen in the numerical example by comparing the exact many-body calculation with the approximate calculation using both Eq. (13) and the SPDM Eq. (11). This is shown in Fig. 8, where a comparison between the three methods is shown. As seen in the figure, the agreement between all schemes is good in general, with substantial differences arising only at the maxima and minima of the current. At these points, the single-particle scheme [Eq. (13)] is closer to the many-body calculation than the SPDM method [Eq. (11)].

VI. SUMMARY

We have proposed an order-N scheme to investigate the dynamics of N non-interacting electrons coupled to one or more baths, and justified it analytically by examining and tracing the full many-body calculation. The main idea is to reduce the equation of motion for the many-body system to a set of effective single-electron equations (Eq. (4)) where both Fermi statistics and dissipation are taken into account via a specific form of relaxation operators (Eq. (5) at $T = 0$; Eq. (20) for $T \neq 0$). We have numerically demonstrated that the proposed method is in excellent agreement with the exact many-body calculation by studying two example. The first example is a system of tight-binding rings at zero temperature, driven out of equilibrium by external radiation. The second example is a linear chain connected at its end to two heat baths held at different temperatures.

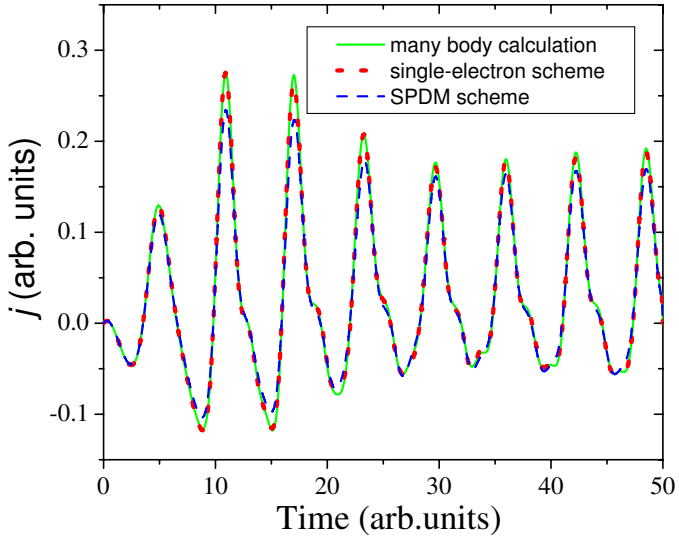

FIG. 8: (Color online) Current excited in a 10-site ring calculated by three different methods as indicated in the figure. This plot was obtained using the same parameter values as in Fig. 1 except $\omega = 1$.

Since, even for non-interacting electrons the inclusion of the Pauli exclusion principle is nontrivial for open quantum systems[21], we believe our scheme can be used in systems where interactions play a relatively minor role such as in graphene[22], quantum point contacts[23], etc. Nevertheless, while the above examples did not include electron-electron interactions, the latter may be included within the framework of stochastic time-dependent current-density functional theory[11], where the interacting many-body problem in the presence of environments is mapped into an effective single-particle problem in the presence of the same environments. Our *ansatz* thus provides a good starting point to solve the corresponding equations of motion with a computational cost that scales only linearly with the number of particles. Such a project is currently underway.

Acknowledgments

We thank S. Saikin for fruitful discussions. This work was funded by the Department of Energy grant DE-FG02-05ER46204.

[1] R. P. Feynman and F. L. Vernon, Ann. Phys. (N.Y.) **24**, 118 (1963).

[2] A. O. Caldeira and A. J. Legget, Ann. Phys. (N.Y.) **149**, 374 (1983).

[3] For a comprehensive review, see, e.g., U. Weiss, *Quantum Dissipative Systems*, Series in Modern Condensed Matter Physics, Vol. 10 (World Scientific, Singapore, 2006).

[4] M. Di Ventra, *Electrical Transport in Nanoscale Systems* (Cambridge University Press, 2008).

[5] N. Bushong *et.al.*, Nano Letters **5**, 2569 (2005).

[6] A. G. Redfield, IBM J. Res. Dev. **1**, 19 (1959).

[7] N. G. Van Kampen, *Stochastic Processes in Physics and Chemistry* (North Holland, Amsterdam, 2001), 2nd ed.

[8] G. Lindblad, Commun. Math. Phys. **48**, 119 (1976).

[9] W. H. Louisell, *Quantum Statistical Properties of Radiation* (Wiley-Interscience, 1990).

[10] An excellent review on the on the use of both the density-matrix methods and the stochastic Schroedinger equation in various problems may be found in, e.g. H. -P. Breuer and F. Petruccione, *The Theory of Open Quantum Systems* (Oxford University Press, Oxford 2002).

[11] M. Di Ventra and R. D'Agosta, Phys. Rev. Lett. **98**, 226403 (2007); R. D'Agosta and M. Di Ventra, cond-mat/08053734.

[12] N. Bushong and M. Di Ventra, cond-mat/0711.0762 (2007).

[13] For the stochastic Schrödinger equations we need to solve for $C_N^M - 1$ elements of the state vector but average over an amount, call it m, of different realizations of the stochastic process.

[14] Yu. V. Pershin and C. Piermarocchi, Phys. Rev. B **72**, 245331 (2005); Phys. Rev. B **72**, 125348 (2005).

[15] K. Nobusada and K. Yabana, Phys. Rev. A **75**, 032518 (2007).

[16] Note that for our choice of parameters the continuity equation is satisfied to a high degree of accuracy.

[17] Y. Dubi and M. Di Ventra, cond-mat/08051415.

[18] See, e.g. B. Ludoph and J. M. van Ruitenbeek, Phys. Rev. B **59**, 12290 (1999), and other references in Ref. 17.

[19] See, e.g., R. Gebauer and R. Car, Phys. Rev. B **70**, 125324 (2004).

[20] C. F. Huang, and K.-N. Huang, Chinese J. Phys. **42**, 221 (2004).

[21] L. Bonig and K. Schonhammer, Phys. Rev. B **47**, 9203 (1993).

[22] H. P. Dahal *et.al.*, Phys. Rev. B **74**, 233405 (2006); H. P. Dahal *et.al.*, cond-mat/0712.2836 (2007).

[23] F. A. Maao and L. Y. Gorelik, Phys. Rev. B **53** 15885 (1996).